



Published in final edited form as:

Nat Neurosci. 2015 June ; 18(6): 917–925. doi:10.1038/nn.4016.

A Transcriptional Reporter of Intracellular Ca²⁺ in *Drosophila*

Xiaojing J Gao¹, Olena Riabinina², Jiefu Li¹, Christopher J Potter², Thomas R Clandinin³, and Liqun Luo^{1,3}

¹Howard Hughes Medical Institute and Department of Biology, Stanford University, Stanford, California, USA

²The Solomon H Snyder Department of Neuroscience, The Johns Hopkins University School of Medicine, Baltimore, Maryland, USA

³Department of Neurobiology, Stanford University, Stanford, California, USA

Abstract

Intracellular Ca²⁺ is a widely used neuronal activity indicator. Here we describe a transcriptional reporter of intracellular Ca²⁺ (TRIC) in *Drosophila*, which uses a binary expression system to report Ca²⁺-dependent interactions between calmodulin and its target peptide. We show that *in vitro* assays predict *in vivo* properties of TRIC, and that TRIC signals in sensory systems depend on neuronal activity. TRIC can quantitatively monitor neuronal responses that change slowly, such as those of neuropeptide F-expressing neurons to sexual deprivation and neuroendocrine *pars intercerebralis* (PI) cells to food and arousal. Furthermore, TRIC-induced expression of a neuronal silencer in nutrient activated cells enhanced stress resistance, providing proof-of-principle that TRIC can be used for circuit manipulation. Thus, TRIC facilitates the monitoring and manipulation of neuronal activity, especially those reflecting slow changes in physiological states that are poorly captured by existing methods. TRIC's modular design should enable optimization and adaptation to other organisms.

INTRODUCTION

Live imaging of Ca²⁺ with fluorescent indicators is a powerful technique for monitoring neural circuit dynamics^{1,2}. Here, we describe a transcriptional reporter of intracellular calcium (TRIC) that captures changes in neuronal activity over long time scales, which complements several limitations of fluorescent indicators. First, functional imaging is usually performed acutely and invasively in restrained animals. As a result, it is difficult to monitor circuits whose activities vary slowly with changes in the physiological state^{3,4}. These circuits often use modulatory neurotransmitters or neuropeptides, and their outputs can cause the same neural network to mediate starkly different behaviors⁵. How the activity

Users may view, print, copy, and download text and data-mine the content in such documents, for the purposes of academic research, subject always to the full Conditions of use:http://www.nature.com/authors/editorial_policies/license.html#terms

Correspondence to: Xiaojing J Gao; Thomas R Clandinin; Liqun Luo.

AUTHOR CONTRIBUTIONS

X.J.G designed, performed, and analyzed the experiments, helped by J.L. during revision. L.L. and T.R.C. supervised the project. O.R. and C.J.P. provided unpublished *nsyb-QF2* line; X.J.G., L.L., and T.R.C. wrote the manuscript, with inputs from all the authors.

of modulatory neurons is regulated under natural conditions remains poorly understood given the absence of suitable tools. Second, because functional imaging and electrophysiology are time-consuming, they have limited capacity to interrogate complex circuits systematically. For instance, serial electron microscopic reconstruction has revealed dozens of prominent connections in one of the flies' visual centers, the medulla⁶. Systematic interrogation of these connections would involve hundreds or thousands of experiments that inactivate specific input neurons, monitor output neurons, and present specific stimuli, which are extremely challenging with existing methods. Third, functional imaging is limited by the field of view accessible to a microscope. Thus, behaviorally relevant changes in neuronal activity in widely distributed brain regions can be difficult to monitor in parallel. Finally, Ca²⁺ imaging only allows visualization of neuronal activity, but does not enable subsequent genetic manipulation of active cells.

An alternative approach to monitoring neural activity is based on the activation of immediate early genes (IEGs), whose expression is increased when neurons are active. Such endogenous transcriptional reporters of activity have been widely used in vertebrate models, and have provided a complementary approach to live imaging of calcium signals⁷. In addition, other effectors have been placed under the control of IEG enhancers/promoters recently for genetic manipulation of active neurons^{8–11}. However, only one IEG has recently been described in fruit flies¹², and alternative methods for monitoring neuronal activity using transcriptional reporters are scarce¹³. Moreover, the mechanism of IEG induction by neuronal activity is still not well understood, hindering the optimization and general application of this strategy.

To address the limitations of calcium imaging experiments, we developed TRIC to integrate changes in Ca²⁺ levels over long periods of time in freely behaving animals. TRIC takes advantage of Ca²⁺-dependent interactions between calmodulin and its target peptides¹⁴, and reports this interaction using a binary expression system (Fig. 1a). TRIC produces a stable signal that can be monitored in fixed tissue, increasing the throughput of experiments that interrogate functional connectivity, and allowing for visualization of neuronal activity in the whole brain. In addition, TRIC allows for subsequent expression of any transgenes, so that one can selectively manipulate active neurons. We have tested TRIC in flies, given the well-established use of split binary systems^{15, 16}, and the potential of combining TRIC with other genetic tools. We provide proof-of-principle experiments using TRIC in cultured cells and in visual, olfactory, and neuromodulatory systems *in vivo*. When applied to *pars intercerebralis* (PI) cells¹⁷, TRIC validates previously known regulatory factors, reveals distinct modes of PI response to different physiological conditions, and enhances stress resistance through the activity-dependent expression of a synaptic transmission blocker.

RESULTS

Selecting TRIC components in cultured cells and flies

To build a transcriptional reporter of intracellular Ca²⁺ levels, we fused calmodulin (CaM) and its target peptide¹⁴ to a transcriptional activation domain (AD) and a DNA-binding domain (DBD), respectively. When CaM binds to its target peptide in the presence of Ca²⁺, the reconstituted transcription factor can express an effector (Fig. 1a). We performed initial

tests of TRIC efficiency in *Drosophila* S2 cells. We induced pulses of Ca^{2+} influx by heat shocking cells transfected with a temperature-gated cation channel, dTrpA1¹⁸. We tested two DBDs, two ADs¹⁶, and three CaM-target peptides¹⁹ (Supplementary Table 1, Fig. 1b, and Supplementary Fig. 1a, 1b). These studies identified that the TRIC version with the best signal-to-noise ratio in cultured cells consists of the codon-optimized GAL4DBD (GAL4DBDo) fused with the CaM-target peptide in CaMKII (MKII), and the p65AD fused with CaM.

In the absence of dTrpA1, CaM/MKII-mediated TRIC expressed little of the co-transfected *UAS-GFP* reporter (Fig. 1b, left). In contrast, heat-induced Ca^{2+} influx through dTrpA1 resulted in robust GFP expression (Fig. 1b, right). The CaM/MKII-mediated TRIC signal was comparable to that of constitutively dimerizing split GAL4¹⁵ (compare Fig. 1b right with Fig. 1c), which was independent of dTrpA1 (Fig. 1c).

To test TRIC *in vivo*, we generated transgenic flies in which *MKII::GAL4DBDo* was expressed using a pan-neuronal promoter (*nsyb*), and *p65AD::CaM* was controlled by *QUAS* from the Q system²⁰. The *p65AD::CaM* was expressed by the *nsyb*-driven transcription factor QF2²¹, and suppressed by the ubiquitously expressed suppressor QS. Adding quinic acid (QA) relieves QS suppression²⁰, allowing us to tune the expression level of TRIC. In the test flies exposed to QA, we observed strong TRIC signal throughout the brain (Fig. 1d) and the ventral nerve cord (Supplementary Fig. 1d). Consistent with the difference *in vitro* (compare Supplementary Fig. 1a right to Fig. 1b right), M13 produced weaker signals than did MKII *in vivo* (compare Supplementary Fig. 1c left to Fig. 1d). Thus, for subsequent experiments, we chose MKII::GAL4DBDo and p65AD::CaM as the core TRIC components.

TRIC signals in the optic lobes depend on visual input

To characterize TRIC's ability to detect changes in neural activity, we started with the optic lobes, which process visual information. In pan-neuronal TRIC flies raised in ambient light, robust signal was detected across the optic lobes (Fig. 2a, "*norPA*+"). By contrast, the signal was nearly abolished (Fig. 2a, "*norPA*-") and quantification) when we introduced a *norPA* mutation, which eliminates phototransduction²².

To test whether sensory experience can modulate the TRIC signal, we raised flies in darkness until eclosion, induced *p65AD::CaM* expression with QA, and then kept animals in ambient light or darkness for three days. However, the ambient light did not significantly elevate TRIC signal (Supplementary Fig. 2a). We hypothesized that, unlike *norPA* mutants, dark-reared flies still have spontaneous photoreceptor activity that could propagate to optic lobe neurons and be detected by TRIC. Such low level of activity might saturate TRIC signal in darkness with an exceptionally stable mCD8::FP reporter. Indeed, we found significant reduction of TRIC signal in dark rearing compared to light exposure, when we used a less stable *nsyb::GFP* reporter²³ (Supplementary Fig. 2b, 2c), or when we restricted reporter availability temporally using a *UAS-FRT-stop-FRT-mCD8::GFP* reporter²⁴ dependent on heat-shock induction of a FLP recombinase (Supplementary Fig. 2d). Thus, with appropriate reporters, TRIC can discriminate between the complete absence of phototransduction, spontaneous activity in darkness, and the response to light.

Next, we used FLP-mediated recombination to regulate expression of the TRIC component *QUAS-FRT-stop-FRT-p65AD::CaM* directly. As we observed before, light exposure induced strong and dense TRIC labeling in the optic lobes after heat-shock-induced onset of *p65AD::CaM* expression (Fig. 2b, “hs + light”). Omitting either light or heat shock markedly reduced TRIC signals (Fig. 2b, “hs”, “light”, and quantification).

We also used FLP-regulated TRIC onset to test whether different visual stimuli trigger distinct TRIC patterns in the medulla, the second optic ganglion. We heat shocked FLP-regulated TRIC flies and then exposed them to darkness, ambient light, moving gratings, or full-field flicker, the latter two stimuli commonly used in visual system studies²⁵. These stimuli increased the overall fluorescent intensity in medulla to different extents (Fig. 2c–2e); and different stimuli appeared to preferentially induce TRIC signal in different layers, evident in individual samples (Fig. 2c) or average heat maps after image registration of multiple flies (Fig. 2d, 2f; see Methods). Thus, with the FLP-regulated temporal, TRIC can report both the overall activity level of the optic lobes, and layer-specific activation within the medulla in response to different visual stimuli.

Characterizing TRIC in the olfactory projection neurons

Many optic lobe neurons use graded potentials. To test whether TRIC can monitor neurons with action potentials, we turned to the spiking olfactory projection neurons (PNs) labeled by *GHI46-QF*²⁰. For flies raised under standard conditions, TRIC labeled PN cell bodies around and dendrites within the antennal lobes (Fig. 3a, “control”); these signals were markedly reduced by genetic ablation of the olfactory receptor neurons (ORNs), the primary presynaptic partners of PNs (Fig. 3a, “ORNs killed” and quantification).

To abolish sensory input acutely, we removed the antennae, which contain the majority of ORNs. An *nsyb::GFP* reporter showed significant signal reduction five days after bilateral antennectomy (Fig. 3b), and this was not due to axon degeneration (Supplementary Fig. 3a). Since ORNs project bilaterally while PNs only innervate the ipsilateral antennal lobe, we tested the consequence of unilateral antennectomy. This manipulation did not reduce PN signal compared to intact flies (Fig. 3b), and signal in the ipsilateral and contralateral antennal lobes were similar (Fig. 3b “left antenna”, Supplementary Fig. 3b), consistent with the reported small differences between the spiking rates in PNs caused by contra- and ipsilateral inputs²⁶. This experiment suggested that single-antenna input saturates PN responses in both hemispheres, reflecting a ceiling in PNs or TRIC. Moreover, a luciferase reporter also detected antennectomy-induced TRIC signal reduction (Fig. 3c, Supplementary Fig. 3c), and the artificial activation of PNs (Supplementary Fig. 3d).

The PNs were characterized for the only reported transcriptional indicator of neuronal activity in flies (CaLexA), a NFAT-LexA chimera whose transcriptional activity is based on the Ca^{2+} -regulated dephosphorylation and nuclear translocation of NFAT¹³. We replaced GAL4DBD with LexADBBD, in order to directly compare the performance of TRIC and CaLexA. We found that LexA-based TRIC labeled PNs broadly and strongly (Supplementary Fig. 4a), matching the performance of GAL4-based TRIC in cell bodies and the neuropil (Fig. 3d). In contrast, CaLexA only labeled two PN classes (Supplementary Fig. 4b). Pan-neuronal CaLexA signal is also much weaker and sparser than TRIC

(Supplementary Fig. 4c, compare to Fig. 1d). This experiment also indicated that TRIC is robust to substitution of the DBD modules.

Monitoring neuromodulatory circuits with TRIC

TRIC relies on the relatively slow process of reporter expression. It is thus well suited for monitoring neuromodulatory circuits, whose activities often vary with an animal's physiological states on a time scale too long for traditional reporters. Having characterized TRIC in the sensory systems, we next turned to investigate its utility in modulatory circuits. We first tested whether TRIC signal can generally be detected in various modulatory neurons. To make TRIC compatible with existing GAL4 drivers, we used *nsyb-MKII::nlsLexADBD* (Fig. 3d, "LexA-based"), together with *p65AD:CaM* driven by UAS. For modulatory neurotransmitters, we tested dopaminergic²⁷, serotonergic²⁸, and tyraminerpic/octopaminergic²⁹ neurons respectively (Supplementary Fig. 5a–5c); we also tested neurons expressing neuropeptide F (NPF)³⁰ (Fig. 4a) and general neuropeptidergic neurons³¹ (Supplementary Fig. 5d). In all cases, TRIC can visualize Ca²⁺ in various proportions of GAL4+ neurons.

We noted that although TRIC signal is high in many modulatory neurons, it is undetectable in others (Fig. 4a, Supplementary Fig. 5a–5d). Indeed, in our initial pan-neuronal TRIC, signals were sparser than would have been expected if every *nsyb+* neuron could convert activity into a TRIC signal (Fig. 1d). Such heterogeneity could reflect different levels of neuronal activity, but could also reflect differences in the ratio between DBD and AD expression. Specifically, in a scenario where DBD components outnumber AD components, even if every AD dimerizes with DBD at high Ca²⁺, the empty DBDs will still compete with transcriptionally active dimers at the genomic binding site, thereby suppressing TRIC signal in a dominant negative manner. We validated this intuition through a computational simulation (see Methods), and observed that while TRIC signal was monotonically increased by increasing the expression of AD (Fig. 4b, left), the signal was first increased and then decreased by increasing DBD expression (Fig. 4b, right). To experimentally test this idea, we constructed *UAS-MKII::nlsLexADBD* flies, and expressed this transgene in the *pars intercerebralis* cells with *ilp2-GeneSwitch*, a GAL4-progesterone-receptor fusion protein whose activity can be adjusted using RU486³² (Supplementary Fig. 5e). The *in vivo* TRIC signal indeed first increased and then decreased as RU486 induction increased (Fig. 4c).

Since DBD/AD stoichiometry was not well controlled when we used the *nsyb* enhancer to express DBD and GAL4/UAS to express AD, we examined NPF neurons as a test for the more balanced expression of both components by GAL4/UAS. TRIC signal was still present in the four neurons originally labeled, albeit at lower levels (Fig. 4d, compare to Fig. 4a); additional signal emerged in the fan-shaped body (Fig. 4d), a brain region implicated in courtship conditioning³³. Based on the simulation, we next added one copy of the AD transgene, which indeed yielded stronger TRIC signal (Fig. 4e). Previous studies have demonstrated that sexual deprivation reduces NPF expression³⁴, but whether such reduction coincides with diminished activity in NPF neurons is unknown. Using TRIC, we observed that sexual deprivation significantly reduced TRIC labeling in an upper layer of the fan-

shaped body (Fig. 4f). Thus, TRIC can also be used to identify changes in neural activity associated with ethologically relevant social experience.

TRIC monitors activity in the *pars intercerebralis* cells

We next focused on the *pars intercerebralis* (PI) cells, one of the most extensively studied modulatory centers in flies. Since PI cells regulate extremely diverse physiological and behavioral processes¹⁷, understanding how these cells integrate relevant cues is an important question. However, the regulation of PI activity is only partially understood (Fig. 5a), mostly reliant on immunostaining assays that measure the somatic retention of Insulin-like peptides (IIPs)¹⁷. We therefore examined whether TRIC can detect known regulatory mechanisms affecting PI activity.

With no basal signal (data not shown), robust TRIC signal in the PI cells of pan-neuronal TRIC adults was detected within one day after QA induction (Fig. 1d), providing temporal control for measuring PI activity. TRIC signals overlap with IIP2 (Fig. 5b) in flies grown on standard food, validating the identity of these cells. Furthermore, the strength of the TRIC signal negatively correlated with IIP2 levels in individual PI cells (Fig. 5b, “Merge” and quantification), consistent with the expectation that higher secretory activity leads to less somatic retention of IIPs.

After tuning TRIC expression level (Fig. 5c and Supplementary Fig. 6a), we found that starvation diminished TRIC signal (Fig. 5c), consistent with the reported PI response to nutrients^{35, 36}. As expected, PI activity was also reduced by deleting *upd2* (Fig. 5c), the fly homologue of the hormone leptin that relays a satiety signal from the fat body to the brain^{35, 36}.

Larval PI cells respond to dietary amino acids but not sugars³⁵, but a similar specificity has not been established in adults. To investigate this, we measured TRIC signals after feeding flies with various combinations of yeast and sucrose. We found that yeast increased the TRIC signal in PI cells, whereas sucrose had no effect either by itself or in combination with yeast (Fig. 5d), consistent with results in larvae. Since sucrose but not amino acid induces *upd2* expression³⁶, we reasoned that *upd2* might not be the sole satiety signal. Indeed, starvation reduced the TRIC signal in PI neurons even in *upd2* mutant (Supplementary Fig. 6b), implying the presence of at least one additional pathway that links satiety to PI activity.

PI cells are also activated by octopamine (OA), a neurotransmitter controlling arousal states^{37, 38}. We validated that OA feeding increased TRIC signal in PI cells, and that an OA antagonist, mianserin, reversed this effect (Fig. 5e). As expected, a null allele of *tyramine β hydroxylase* (*tbh*)³⁹, the gene necessary for OA synthesis, also decreased PI activity (Fig. 5f).

In summary, using TRIC, we have corroborated regulations of PI activity inferred in previous studies. TRIC also provided new information regarding the nutritional requirements for PI activity in adults, and suggested signaling pathways other than Upd2/leptin that mediate the PI response to satiety (Fig. 5a).

Enhancing the dynamic range of TRIC through mutagenesis

Although we have validated TRIC in PI cells, the small effect sizes (e.g., Fig. 5d, 5e) might limit further quantitative analysis. To optimize TRIC, we screened every alanine variant of MKII in S2 cells. Since the signal of M13 *in vivo* was too low and the baseline of MKII too high, we reasoned that the useful variants would show signals intermediate between M13 and MKII in the presence of dTrpA1 (Fig. 6a; data not shown). To examine the relation between TRIC signal and Ca^{2+} concentration, we simultaneously measured the intensity of a fluorescent Ca^{2+} indicator GCaMP6m⁴⁰ and a *UAS-tdTomato* reporter expressed by TRIC (see Methods). dTrpA1-mediated Ca^{2+} influx induced F/F of about 100% (Fig. 6b; data not shown), comparable to *in vivo* physiological responses⁴⁰. Compared to the no-dTrpA1 control, TRIC signal underwent a 2.2-fold increase with the original MKII, whereas M13 resulted in a signal too weak to be significant (Fig. 6b). As an example for the alanine mutants, MKIIK11A reduced both the baseline and the induced TRIC signals compared to MKII, but increased the fold of induction to 3.6 (Fig. 6b).

To better understand the behavior of the MKIIK11A variant, we estimated its affinity to CaM based on *in silico* alanine scan (Supplementary Fig. 7d, see Methods), and then simulated its dose response. In the simulation, MKIIK11A lowered the TRIC signal (Supplementary Fig. 7a, left), although the MKII and MKIIK11A dose-response curves were almost identical after normalizing to their respective maximums (Supplementary Fig. 7a, right). Thus, reduced affinity alone is insufficient to account for the increased induction ratio (Fig. 6b), unless some form of nonlinearity transforms the proportional decrease of signal by K11A. One possible source of nonlinearity is competition from endogenous CaM and its target peptides. Assuming the simplest case that endogenous CaM and its target peptides are expressed in equal concentrations, and that the endogenous peptides have the same affinity for CaM as MKII, simulation revealed that TRIC signal decreased as the number of endogenous competitors increased (Supplementary Fig. 7b, left), which again preserved the shape of the curve (Supplementary Fig. 7b, right). However, when the K11A variant was simulated in the presence of competition, the mutation caused a rightward shift of the response curve (Supplementary Fig. 7c), consistent with the lower sensitivity and higher induction rate of this variant than MKII. This likely explains the performance of the alanine variant, and suggests a mechanism to account for heterogeneity of TRIC signals in different neuronal types.

Based on our *in vitro* and *in silico* analyses, we tested 5 intermediate variants in PI cells (data not shown). Of these, MKIIK11A reduced PI TRIC signal in both fed and starved flies, with a larger effect on the latter. Consequently, while the TRIC signal was still robust in fed flies, it was negligible after starvation (Fig. 6c), and the ratio of TRIC signals between the fed and starved states quadrupled that of the original MKII (16 fold in Fig. 6c, compared to 3.7 fold in Fig. 5c, also see Fig. 6b for comparison).

We took advantage of this variant to measure the temporal characteristics of TRIC signal in PI cells. Shortening food induction by half reduced TRIC signal by half (Supplementary Fig. 6c), suggesting that the signal accumulates linearly over time. To measure signal perdurance, after one-day induction of PI activity by food, the flies were either examined

immediately or starved for 1 or 2 days before dissection, where the half-life of TRIC signal was determined to be 0.55 day (Supplementary Fig. 6d).

TRIC reveals distinct modes of PI activity regulation

Signal induction by yeast and OA was also greatly improved by MKIIK11A (Supplementary Fig. 6e, 6f, compared to Fig. 5d, 5e), which allowed us to quantitatively compare PI's dose responses to yeast and OA exposure. PI TRIC signal increased linearly with yeast concentration (Fig. 6d). In contrast, as the OA concentration rose, the TRIC signal plateaued at a level much lower than the maximal signal induced by yeast (Fig. 6e, compared to Fig. 6d). One possible explanation for this non-linear response was that OA uptake was simply saturated. In this scenario, 10 or 20 mg/mL OA would result in the same amount of OA acting on its receptors in PI cells, and their effects should be equally inhibited by mianserin. To test this, we used an intermediate mianserin dose (Supplementary Fig. 6g, left), and found that 10 mg/mL OA induced a smaller TRIC signal than 20 mg/mL OA (Supplementary Fig. 6g, right). Thus, OA uptake was not saturated under these conditions, suggesting that the observed saturation of the TRIC signal took place at or downstream of the OA receptors.

The difference in dose-response curves suggested that yeast and OA activate PI cells through separate pathways. To test this notion, we asked whether the response to 5% yeast, which induced PI activity higher than the ceiling of OA response (Fig. 6d, 6e), could be further augmented by adding OA. Indeed, adding 10 mg/mL OA increased the signal induced by 5% yeast (Fig. 6f). In summary, nutrients and OA regulate PI activity through separate pathways and display distinct dose responses.

TRIC variants cover a wide range of neural activity

Our characterization of TRIC so far contains several variants of TRIC. We used yeast-regulated PI activity to quantitatively compare these variants. All the subsequent data were normalized to the TRIC signal of MKIIK11A::GAL4DBDo driving mCD8::GFP, exposed to 10% yeast.

Compared to MKIIK11A::GAL4DBDo (black in Fig. 6g), the original MKII::GAL4DBDo driving mCD8::GFP displayed a high baseline with plain agar, and was saturated using 2% yeast (blue in Fig. 6f). Replacing GAL4DBDo with nlsLexADBDo led to a more gradual elevation of signal as yeast concentration increased (purple in Fig. 6g); replacing the mCD8 reporter with nsyb::GFP greatly reduced the signal, while also increasing the range of signal induction (golden in Fig. 6g, compare to blue). Finally, combining the MKIIK11A mutation with nlsLexADBDo, we detected no TRIC signal except at the highest yeast concentration, 10% (orange in Fig. 6g). Taken together, these comparisons reveal that MKII::GAL4DBDo driving mCD8::GFP is the most sensitive reporter, and MKIIK11A::nlsLexADBDo driving mCD8::GFP is the most stringent. Collectively, these variants display a wide dynamic range that can be selected by users in their neurons of interest.

A TRIC-driven synaptic blocker enhances stress resistance

Having achieved a high signal-to-baseline ratio of the MKIIK11A variant in PI cells, we tested whether TRIC-based expression of an effector can be used to manipulate circuit function. We used TRIC to express *shits¹*, a widely used mutant dynamin that disrupts synaptic transmission at restrictive temperature⁴¹. We focused on validating a well-characterized phenotype in which inactivating PI cells enhances stress resistance, as measured by survival upon starvation⁴².

All *TRIC > shits¹* flies were first kept at 25 C on food for two days. The experimental group (red in Fig. 6h) was exposed to QA on the first day, so that *shits¹* was expressed on the second day in PI cells due to food-induced activity; the control group (cyan in Fig. 6h) was exposed to QA on the second day, so that there was minimal PI activity to follow the onset of TRIC and no *shits¹* expression. All flies were then starved at the restrictive temperature for *shits¹*. The experimental group survived significantly longer than the control group (Fig. 6h, upper panel). Further controls confirmed that there was no difference in survival in the absence of the *shits¹* transgene (Fig. 6h, lower panel). The phenotype is like due to expression in PI cells rather than elsewhere in the brain, since when we visualized TRIC signal in the whole brain under these conditions, the only notable difference between the control and the experiment was in the PI cells (Supplementary Fig. 6h). TRIC can thus mediate neural-activity-dependent expression of genetic effectors that manipulate circuit function.

DISCUSSION

Using cultured cells and multiple *in vivo* assays, we demonstrated that TRIC reports changes in Ca²⁺ levels under diverse conditions in visual, olfactory, and neuromodulatory systems. We provided quantitative assessments for choosing TRIC variants with appropriate sensitivity and stringency, and proof-of-principle that TRIC can be used to express a circuit manipulator. Thus, TRIC provides a useful complement to functional Ca²⁺ imaging by integrating changes in activity over long periods of time, and offering genetic access to neurons based on their activity.

Comparing TRIC with other methods

Vertebrate immediate early genes (IEGs), evolved to express in a high signal-to-baseline ratio in response to neuronal activation, are widely used to report neuronal activity⁷. However, since they rely on endogenous signaling networks, their response properties and cell-type biases are difficult to modify. TRIC can be considered a rationally designed IEG, by exogenously introducing a protein-peptide interaction to detect Ca²⁺. The modular design of TRIC renders it more amenable to optimization. TRIC reports a rise in nuclear Ca²⁺ levels, which has previously been used to monitor pan-neuronal activity in *C. elegans*⁴³, and also accompanies neuronal activation in mammalian neurons likely shuttled by Ca²⁺-binding proteins⁴⁴. Our experiments indicate that nuclear Ca²⁺ correlates with activity in diverse neuronal classes in flies. It is likely that not all cell types have the same efficiency in converting cytoplasmic Ca²⁺ signal to nuclear Ca²⁺ signal. Thus, TRIC efficiency and optimization may differ for different neuronal types.

While this manuscript was in review, a Ca^{2+} integrator (CaMPARI) was reported, where the UV-conversion of emission spectrum of a fluorescent protein was engineered to be contingent on Ca^{2+} concentration⁴⁵. CaMPARI can capture neuronal activity on a shorter time scale than TRIC or IEG. However, access of neurons to UV may limit the use of CaMPARI in deep tissues, at least in large animals, whereas TRIC and IEG report neuronal activity in the entire nervous system non-invasively. Notably, unlike CaMPARI or IEG, TRIC offers genetic access to active neurons, allowing activity-based circuit manipulation (e.g. Fig. 6h).

Tuning the parameters of TRIC

Our results underscore the importance of optimizing TRIC for specific neuronal types. In this study, we have optimized TRIC for multiple cell types, and have described many variants that can help users in other cells (Fig. 6g, Supplementary Table 2). We recommend that users begin with CaM/MKII-mediated TRIC (Fig. 1, 5, 6g) in their neurons of interest. If TRIC signal is detected, the users can attempt QA-mediated (Fig. 5, 6) or FLP-mediated (Fig. 2) regulation of the timing of TRIC onset. The signal-to-baseline ratio can be further improved by titrating expression of TRIC using QA (Fig. 5 and Supplementary Fig. 6), choosing reporters with different stabilities (Fig. 3, 6g, Supplementary Fig. 2), or switching to nlsLexADBD0 (Fig. 3, 6g) or the MKI1K11A variant (Fig. 6, Supplementary Fig. 8). Stoichiometry can also be leveraged to boost TRIC signal (Fig. 4).

With the current version of TRIC, the signal accumulates and decays over many hours (Supplementary Fig. 6c, 6d). To detect shorter periods of neuronal activity, an important future goal is to increase signal strength while avoiding saturation by basal Ca^{2+} concentrations. One solution to this problem would be to restrict TRIC to a narrower time window than offered by the QA- or the FLP-mediated strategy. For example, TRIC could be split into DBD-X, Y-target-peptide, and CaM-AD, where X and Y are two interacting modules controlled by light⁴⁶. One can then synchronize TRIC with a specific manipulation, or even trigger TRIC repetitively with specific behavioral features using feedback from automated tracking⁴⁷. To preserve phasic information about neuronal activity, reporters with faster decays than CD8::GFP (Supplementary Fig. 2c) can be used, or the TRIC components can be destabilized with tags for protein degradation. Since the current TRIC can interact with endogenous CaM and their target peptides, another important direction is to “isolate” TRIC by co-engineering the CaM and MKII components to lose binding to their endogenous partners but maintain their mutual interaction⁴⁸. Future TRIC optimization can be achieved using high throughput screens in cultured cells, which can predict *in vivo* performance (Fig. 1, 5, 6, and Supplementary Fig. 1).

The modulation of PI activity

Previous studies^{17, 35, 36} used Ilp2 immunostaining, epitope-tagged Ilp2, or a secreted GFP as indirect indicators of PI activity. We validated the major conclusions of these studies using TRIC. After enhancing the dynamic range of TRIC, we have gained additional insight into how PI activity is regulated. In particular, since PI cells affect diverse processes, how do these cells determine their output according to all relevant inputs? For example, an animal may encounter conflicting metabolic needs, such as conserving energy versus

defending territory in an impoverished environment. Our nutrient/OA comparison could be viewed as a minimal model of such a dilemma, since OA contributes to arousal, and is necessary for “fight or flight” in insects^{38,49}. We showed that PI cells exhibited graded yet more readily saturated response to such events. In contrast, the linear PI response to nutrients extends over a wider range. These distinctions, plus the additive interaction between yeast and OA, point to the independent operation of these two categories of inputs. To further survey the input landscape, one can genetically manipulate candidate receptors autonomously or candidate upstream neurons non-autonomously, while monitoring PI activity using TRIC.

Applying TRIC to other systems

The physiological states of flies can change over hours to days, and can be accompanied by changes in the activities of neurons expressing modulatory neurotransmitters^{3,4} or neuropeptides^{17,34}. While previous work has focused on the targets of modulatory neurotransmitters, inputs to these cells remain largely unknown. In addition, there are ~75 predicted neuropeptides in flies, only a small subset of which have been examined⁵⁰. TRIC can be applied to neurons expressing specific transmitters or neuropeptides, and tested in different physiological states (e.g., the NPF neurons in Fig. 4). We note that the current TRIC variants might not fit the dynamic range of all neuronal types, and it might be necessary to test other AD/DBD ratios or other MKII mutants following our examples of optimization for PI cells.

Finally, TRIC can report a rise of intracellular Ca²⁺ that accompanies any cellular, developmental, or physiological processes in flies and can be adapted for similar use in other model organisms. TRIC modules can be introduced as transgenes or by viral vectors, and specific stoichiometry can be achieved by specifying the number of AD and DBD sequences in multi-cistronic constructs. TRIC expression can be made contingent on recombinase or other binary systems in model organisms such as mice where many Cre lines are available for spatiotemporal control, which can help refine activity monitoring and circuit manipulation in specific cell types.

ONLINE METHODS

DNA constructs described in this manuscript will be available at Addgene. Transgenic flies will be available at Bloomington Stock Center.

Recombinant DNA Construction

DNA construction was made using standard cloning methods. PCR amplifications were conducted with high-fidelity Phusion polymerase (NEB #M0535). The insertions were all verified by sequencing. Several intermediate constructs were not referred to in the paper.

pAC-dTrpA1—The *dTrpA1* sequence was amplified from *pUAST-dTrpA1*¹⁸ using primers CGATGCGGCCGCAACATGACTTCGGGCGACA and CGATGGCGCGCCTACATGCTCTTATTGAAGCTCAGG, and cloned into pP_{AC5C}-PL¹⁵ using NotI/AscI.

pAC-GCaMP6m—The GCaMP sequence was amplified using primers ATCCGATCTGCGGCCGCAAATGGGTTCTCATCATCA and ATCGGTTATGGCGCGCCTCACTTCGCTGTCATCATT, and cloned into NotI/AscI-digested pP_{AC5C}-PL using In-Fusion reaction (Clontech #638910).

pAC-VP16AD::CaM—The *CaM* sequence was amplified from GCaMP3⁵¹ using primers CGATACTAGTGACCACTGACTGAAGAGCAGATCG and CGATGGCGCGCCTTACTTCGCTGTCATCATTTGTACAACTCT, replacing the leucine zipper in *pAC-VP16AD::Zp*¹⁵ using SpeI/AscI.

pAC-p65AD::CaM—The *p65AD* sequence was amplified from *pBPp65ADZpUw*¹⁶ using primers CGATGCGGCCGCAAACATGGATAAAGCGGAATTAATTCC and CTCCGCTAGCGGAGCTTATCT, replacing the *VP16AD* in *pAC-VP16AD::CaM* using NotI/NheI.

pAC-M13::GAL4DBD—The *M13* sequence was amplified from GCaMP3⁵¹ using primers CGATGCGGCCGCCACCATGGGTTCTCATCA and CGATTCTAGATGAGCTCAGCCGACCTATAGCT, digested with NotI/XbaI, and used to replace the leucine zipper in *pAC-Zp::GAL4DBD*¹⁵ between NotI/NheI.

pAC-M13::GAL4DBDo—The *GAL4DBDo* (codon-optimized) sequence was amplified from *pBPZpGAL4DBDUw*¹⁶ using primers GGAGGTACTAGTATGAAGCTGCTGAG and CGATGGCGCGCCTTACGATACCGTCAGTTGCCGT, replacing the *GAL4DBD* in *pAC-M13::GAL4DBDo* using SpeI/AscI.

pAC-MKII::GAL4DBD—The *MKII* (codon-optimized) sequence¹⁹ was generated by annealing oligos
GGCCGCCACCATGTTTAATGCGCGGCGCAAGCTAAAGGGAGCCATACTTACGAC
AATGTTG GCGACCAGAAATTTTCGG and
CTAGCCGAAAAATTTCTGGTCGCCAACATTGTCGTAAGTATGGCTCCCTTTAGCT
TGCGCCGC GCATTAAACATGGTGGC, and ligated between the NotI/NheI sites on *pAC-Zp::GAL4DBD* to replace *Zp*.

pAC-skMLCKN5A::GAL4DBD—The *skMLCKN5A* (codon-optimized) sequence¹⁹ was generated by annealing oligos
GGCCGCCACCATGGGCGCTGGAAGAAGGCCTTCATCGCCGTGAGCGCCGCCA
ACCGCTTC AAGAAGATCAGCG and
CTAGCGCTGATCTTCTTGAAGCGGTTGGCGGCGCTCACGGCGATGAAGGCCTTC
TTCCAGCG GCCCATGGTGGC, and ligated between the NotI/NheI sites on *pAC-Zp::GAL4DBD* to replace *Zp*. We chose the N5A mutation that increases CaM-skMLCK affinity⁵².

pAC-MKII::GAL4DBDo—The *GAL4DBDo* (codon-optimized) sequence was amplified from *pBPZpGAL4DBDUw*¹⁶ using primers GGAGGTACTAGTATGAAGCTGCTGAG and CGATGGCGCGCCTTACGATACCGTCAGTTGCCGT, replacing the *GAL4DBD* in *pAC-MKII::GAL4DBDo* using SpeI/AscI.

Alanine variants of *pAC-MKII::GAL4DBDo*—For alanine variant of each residue, the corresponding codon in MKII was changed to GCC. For example, the *MKIIK11A* sequence was generated by annealing oligos
 GGCCGCCACCATGTTTAATGCGCGGCGCAAGCTAgccGGAGCCATACTTACGACA
 ATGTTGGC GACCAGAAATTTTTTCGG and
 CTAGCCGAAAAATTTCTGGTCGCCAACATTGTCGTAAGTATGGCTCCggcTAGCT
 TGCGCCGC GCATTAACATGGTGGC (the replaced codon in lowercase), replacing the *MKII* in *pAC-MKII::GAL4DBDo* using NotI/NheI.

pQUAST-p65AD::CaM—The *p65AD::CaM* sequence was amplified from *pAC-p65AD::CaM* using primers CGATAGATCTCAACATGGATAAAGCGGAATTAATTCC and CGATCTCGAGTTACTTCGCTGTCATCATTTGTACAACTCT, and cloned in to *pQUAST*²⁰ using BglII/XhoI.

pattB-nsyb-M13::GAL4DBDo—The *M13::GAL4DBDo* sequence was amplified from *pAC-M13::GAL4DBDo* using primers
 CGATGAATTCACCATGGGTTCTCATCATCATC and
 CGATGACGTCTTACGATACCGTCAGTTGCCGT, replacing the *GAL4* in *pattB-nsyb-GAL4*²¹ using EcoRI/AatII.

***pattB-nsyb-MKII::GAL4DBDo* and the alanine variants**—The *MKII::GAL4DBDo* sequence was amplified from *pAC-MKII::GAL4DBDo* using primers
 CGATGAATTCACCATGTTTAATGCGC and
 CGATGACGTCTTACGATACCGTCAGTTGCCGT, replacing the *GAL4* in *pattB-nsyb-GAL4* using EcoRI/AatII. For the alanine variants, the corresponding codon in the 5' primer is changed accordingly.

pQUAST-FRT-stop-FRT-p65AD::CaM—The *FRT-stop-FRT* sequence was amplified from *pQUAST-FRT-stop-FRT-mCD8::GFP*²⁰ using primers
 TAACAGATCTGAGGGTACCCG and CGATAGATCTGGTACCCAGCTTCAAAGC, and cloned into *pQUAST-p65AD::CaM* using BglII. The correct orientation was selected after sequencing.

pAC-MKII::nlsLexADBDo—The *nlsLexADBDo* (codon-optimized) sequence was amplified from *pBPnlsLexA-p65Uw*¹⁶ using primers
 CGATACTAGTCCACCCAAGAAGAAGCG and
 CGATGGCGCGCCTTACAGCCAATCTCCGTTGC, replacing the *GAL4DBD* in *pAC-MKII::GAL4DBDo* using SpeI/AscI.

pattB-nsyb-MKII::nlsLexADBDo—The *MKII::nlsLexADBDo* sequence was amplified from *pAC-MKII::nlsLexADBDo* using primers CGATGAATTCACCATGTTTAATGCGC and CGATGACGTCTTACAGCCAATCTCCGTTGC, replacing the *GAL4* in *pattB-nsyb-GAL4* using EcoRI/AatII.

pattB-nsyb-MKIIK11A::nlsLexADBDo—The *MKII::nlsLexADBDo* sequence with the desired point mutation was amplified from *pattB-nsyb-MKII::nlsLexADBDo* using primers

ATCGACAGCCGAATTCACCATGTTTAATGCGCGGCGCAAGCTAGCCGGAGCCAT ACTTACGA CAA and CTTTAGTTCGACGGTATCGATAG, and cloned into EcoRI/AatII-digested *pattB-nsyb-GAL4* using In-Fusion reaction.

pUAST-attB-p65AD::CaM—The *p65AD::CaM* sequence was digested from *pQUAST-p65AD::CaM* using EcoRI/XhoI and ligated into the corresponding sites in *pUAST-attB*⁵³.

pUAST-attB-MKII::nlsLexADBDo—The *MKII::nlsLexADBDo* sequence was amplified from *nsyb-MKII::nlsLexADBDo* using primers ATTCGTAAACAGATCTCACCATGTTTAATGCGC and TAGAGGTACCCTCGAGTTACAGCCAATCTCCGTTG, and cloned into BglII/XhoI-digested *pUAST-attB*⁵³ using In-Fusion reaction.

S2 Cell Transfection, Manipulation, and Quantification

S2 cells were maintained in Schneider's Insect Medium (Sigma #S0146), supplemented with 10% heat inactivated fetal bovine serum (FBS) and antibiotics. The cells were cultured in a 25 °C air incubator. The DNAs for transfection were mini-prepped (Qiagen) and their concentrations were measured with a NanoDrop spectrophotometer (Thermo Scientific). All transfections were performed with Effectene Reagent (Qiagen) following the manufacturer's protocol.

The qualitative images were collected from 96-well plates. For each well, 25 ng of each plasmid was used and supplemented with carrier plasmid so that the total amount of DNA was always 100 ng. The transfected cells were kept in the 25 °C incubator for 12h, and then transferred onto a thermal cycler (MJ research, #PTC-200). The heat-shock program was 3' at 35 °C and 27'' at 22 °C without lid heating, repeating for 36 hours. The cells were then imaged under a fluorescent microscope using the same parameters.

Quantitative comparisons of Ca²⁺ signals using a fluorescence indicator GCaMP6m and a TRIC reporter tdTomato were performed on chambered cover glasses (Fisher Scientific 12565470) using the adherent S2R+ cells. For each chamber, 15 ng of DBD, 10 ng of AD, 20 ng of UAS-tdTomato, and 75 ng of GCaMP6m plasmids were used; the stimulus conditions involved 30, 15, and 15 ng dTrpA1 plasmid for MKII, MKI1K11A, and M13 respectively, supplemented with carrier plasmid so that the total amount of DNA was always 150 ng. The transfected cells were kept in the 25 °C incubator for 8h, and then transferred onto a thermal cycler with the aforementioned heat-shock program for 18h. The cells were then imaged on an inverted spinning disk microscope at room temperature. For each chamber, we first imaged tdTomato signal in 7 randomly selected fields of views. We then imaged GCaMP signal at exactly the same positions for 10 frames at 0.1 Hz, and delivered 200 μL 45 °C S2 medium to the 200 μL medium already in the chamber to reach approximately 35 °C. The baseline image of GCaMP was the mean of the first five frames; these signals were used to segment the cells with custom Matlab scripts. For each cell, its mean intensity of TRIC signal was normalized to its mean baseline intensity of GCaMP to account for intercellular variability of transfection and expression; the heat-induced peak signal of GCaMP was the highest intensity among the last five frames, and F/F was

calculated as (peak-baseline)/baseline. Each data point represents the mean of all cells from duplicated wells.

***Drosophila* Genetics and Manipulations**

Fly husbandry—In addition to the flies generated with standard P-element-mediated or site-directed transgenesis for this study (Supplementary Table 2), the following flies were used (annotated with Bloomington Stock # when available): *tubP-QS* (30022), *UAS-mCD8::RFP* (32229), *lexAop2-mCD8::GFP* (32229), *UAS-mCD8::GFP* (5137), *norpA*²⁰²², *UAS-nsyb::GFP* (9263), *UAS-GFP::RpL10A* (42683), *hsFLP* and *UAS>CD2, y +>CD8::GFP*²⁴, *hsFLP122*⁵⁴, *GHI46-QF* (30015), *pebbled-GAL4*⁵⁵, *ey-FLP* (5580), *UAS>w+>RTA*⁵⁶, *UAS-luciferase* (gift from G. Dietzl), *GHI46-LexA*⁵⁷, *LexAop2-dtrpA1* (gift from Rubin G.), *upd2*⁵⁸, *UAS-CaLexA* and *LexAop-mCD8::GFP::2A::mCD8::GFP*¹³, *Tbh^{MI8}*⁵⁹, *ple-GAL4* (8848), *trh-GAL4* (38388), *tdc2-GAL4* (9313), *npf-GAL4* (25681), *dimm-GAL4* (25373), *ilp2-GeneSwitch*³², *orco-GAL4* (26818), *UAS-shi^{ts1}*⁴¹, *nsyb-QF2*²¹.

We used the “cornmeal, molasses, and yeast medium” listed on Bloomington website. All experimental flies were raised in a dark 25 °C incubator unless specified, and collected 1–5 days after eclosion. For QA induction, 75 mg QA (or 20 mg for all PI experiments) was dissolved in 300 µL water, evenly applied to the surface of 10 mL food in a small vial, and let dry overnight. Females were used throughout the experiments, except for Fig. 2a, 4a, 4d, 4e, 5c, 5f, 6c, and Supplementary Fig. 6.

Visual system—For the experiments that contain *tubP-QS* in the cross, the collected flies were transferred onto QA food, and remained there for 3 days. They were either placed on the benchtop exposed to “ambient light” or enclosed in a dark cardboard box. We quantified the fluorescence in the anterior half of the optic lobes, where we drew identical rectangles in the counterstaining channel and then measured fluorescent intensity in the signal channel.

For the FLP-mediated experiments, flies were raised at 18 °C. Young adult flies were exposed to 3 10-minute heat shocks at 37 °C, with 2 hour intervals in between. They were then kept at room temperature for 4 days, the first of which always in dark, and the last 3 of which subject to different visual experiences. The specific visual stimulations were programmed with Psychtoolbox in Matlab (Mathworks) and delivered with a high-speed monitor designed for optomotor response⁶⁰. The moving gratings were full-contrast sine waves with a spatial period of 2.5 cm and a frequency of 20 Hz, reversing direction every 10 seconds. The full-field flicker consisted of 8-second blocks of 20 Hz flipping between black and white, interspersed with 2 seconds of gray.

Olfactory system—For the PN experiments, antennal removal was performed with forceps while the flies were anesthetized with CO₂, and the control flies were exposed to CO₂ for the same duration. TRIC signal was measured 5 days after surgery. For the artificial activation with dTrpA1, experiment and control flies were collected in 0.6 mL Eppendorf tubes. Each tube contained 2–3 flies, 50 µL food at the bottom, and sealed with cotton instead of the plastic cap for ventilation. The cotton was soaked with 100 µL water to prevent dehydration. The heat-shock program was conducted on a thermal cycler (MJ research, #PTC-200), with 3” at 37 °C and 27” at 22 °C, repeating for 24 hours.

To measure luciferase activity, 3-fly groups were ground up in Glo lysis buffer (Promega #E2661), and assayed with Steady-Glo (Promega #E2510) system following the manufacturer's protocols. The luminosity was measured in 96-well plates using a VICTOR² multilabel counter (PerkinElmer #1420-018).

NPF neurons—We collected males 0–2 days old, and then housed them for 4 days either by themselves or with an equal number of virgins with daily replenishment. We quantified fluorescent intensity in the topmost layer in the fan-shaped body that has TRIC signal, and only included the anterior part down to the slice where the layer splits into bilateral lobes. We combined data from two independent experiments by aligning the overall mean.

PI cells—The collected flies we placed on QA food for one day, and on the second day they were exposed to different conditions. The “starve” condition was an empty vial with water-soaked Kimwipe. For each yeast/sucrose feeding experiment, the specified amounts were added to 10 mL water in a small vial, in addition to 0.15 g agar. They were heated in a microwave oven until boiling, and left at room temperature to solidify. For each OA/mianserin experiment, the specified amounts were freshly dissolved in 1.5 mL water, and applied to a Kimwipe in an empty vial. The yeast-OA interaction experiments were water-based, where the dry yeast was boiled with water, and the supernatant after centrifugation was obtained to apply to a Kimwipe.

Computational Alanine Scanning of MKII

We also explored the potential of *in silico* optimization. To do this, we used the Robetta server to simulate the change of binding energy caused by each alanine mutation in MKII⁶¹. While no correlation was found between *in vitro* and *in silico* alanine scan mutagenesis when we considered all variants (data not shown), significant correlation emerged when we excluded variants in which a charged residue was mutated to alanine (Supplementary Fig. 7d). This is consistent with previous knowledge that Robetta performs better with non-charged residues⁶¹, and suggests that future optimization may be aided by a computational exhaustion of the parameter space.

For the simulation in the next section, we estimated the affinity of MKIIK11A, a mutation to a charged residue, as follows. In the S2 cell assay, signal from the MKIIK11A variant belongs to “Rank 2”, so we estimated the change of binding energy caused by K11A, as the mean of the Robetta predictions for the three non-charged residues in the same “TRIC signal = 2” column (Supplementary Fig. 7d). As a result, $K_{CaM/MKIIK11A}/K_{CaM/MKII} = 1.838$.

Simulating TRIC signals

The TRIC signal in Fig. 4b and Supplementary Fig. 7 was calculated as follows:

Independent Variables— $[Ca^{2+}]$: Ca^{2+} concentration (normalized to the dissociation coefficient between Ca^{2+} and CaM).

$[AD]$: the total number of AD::CaM proteins (normalized to the dissociation coefficient between DBD and its target sequence).

[DBD]: the total number of peptide::DBD proteins (normalized to the dissociation coefficient between DBD and its target sequence).

[CaM]: the total number of endogenous CaM (normalized to the dissociation coefficient between DBD and its target sequence).

[peptide]: the total number of endogenous CaM-target peptide (normalized to the dissociation coefficient between DBD and its target sequence).

Parameters— $K_{CaM/peptide}$, $K_{CaM/MKII}$, $K_{CaM/MKIIK11A}$: dissociation coefficients between Ca^{2+} -bound CaM and endogenous target peptides, MKII, and MKIIK11A, respectively (normalized to the dissociation coefficient between DBD and its target sequence).

Initialization—[DBD] = 1.5 (for “1 DBD”), [AD] = 1.5 (for “1 AD”), [CaM] = 1.5 (for “1 × competition”), and [peptide] = 1.5 (for “1 × competition”).

We arbitrarily set $K_{CaM/MKII} = 1$, and the corresponding $K_{CaM/MKIIK11A} = 1.838$ according to the estimation in the “computational alanine scanning” section.

Assumptions— $[Ca^{2+}] \gg [AD] + [CaM]$.

Complete cooperativity between the four Ca^{2+} -binding sites on CaM, as illustrated in Fig. 1a. [DBD] \gg its target sequence.

$$K_{CaM/peptide} = K_{CaM/MKII}$$

Calculations

$$[CaM \bullet Ca^{2+}] = ([AD] + [CaM]) \times [Ca^{2+}]^4 / (1 + [Ca^{2+}]^4)$$

find the solution to $[DBD \bullet CaM \bullet Ca^{2+}]$ following five equations:

$$[DBD]_{free} \times [CaM \bullet Ca^{2+}]_{free} / [DBD \bullet CaM \bullet Ca^{2+}] = K_{CaM/MKII} \text{ (or } K_{CaM/MKIIK11A} \text{)}$$

$$[DBD]_{free} + [DBD \bullet CaM \bullet Ca^{2+}] = [DBD]$$

$$[peptide]_{free} \times [CaM \bullet Ca^{2+}]_{free} / [peptide \bullet CaM \bullet Ca^{2+}] = K_{CaM/peptide}$$

$$[peptide]_{free} + [peptide \bullet CaM \bullet Ca^{2+}] = [peptide]$$

$$[CaM \bullet Ca^{2+}]_{free} + [DBD \bullet CaM \bullet Ca^{2+}] + [peptide \bullet CaM \bullet Ca^{2+}] = [CaM \bullet Ca^{2+}]$$

then:

$$\text{signal} = [DBD \bullet CaM \bullet Ca^{2+}] / (1 + [DBD]) \times [AD] / ([AD] + [CaM])$$

Imaging and Image Processing

Immunohistochemistry—Brains were dissected and stained following standard procedures⁶². Primary antibodies: Mouse nc82 (DSHB mAbnc82, 1:30), Chicken anti-GFP (Aves Labs GFP-1020, 1:1000), Rabbit anti-dsRed (Clontech 632496, 1:500). Brains from the same condition were processed within the same tube.

Imaging brains—Images were taken on LSM 510 or 780 confocal microscopes with 20X objectives (Zeiss). For experiments in the same panel, we adjusted the gain so that the sample with the strongest signal barely saturates the dynamic range of the PMT, and imaged all the brains with the same settings and as close as possible time-wise. We did not adjust the offset.

Image analysis—Images were analyzed with Fiji. For fluorescence intensity quantification, the Z stacks of the sum of TRIC signals were generated. We then manually selected the region of interest (see details under the subheadings for each manipulation) to measure the total intensity.

Comparisons were made between data collected either from parallel experiments, with exactly the same master mix of solutions, timeline, and imaging conditions, or from different batches of experiments normalized to common controls. For example, data for Fig. 6g were collected separately, but within each batch there was always one group of *MKIIK11A::GAL4DBD* > *mCD8::GFP* exposed to 10% yeast, whose signal intensity served as the common denominator. Each experiment was repeated at least twice, and we only presented qualitatively consistent results. The data passes Jarque-Bera test whenever normality was assumed.

Custom Matlab scripts were used to assist the averaging of medulla images. The confocal stacks were loaded into Matlab. For each sample, we visually selected a slice corresponding to the same anterior-posterior position according to the nc82 counterstain pattern. Matlab then masked the image using a user-defined threshold. We manually selected the block of neuropil corresponding to the medulla, and Matlab traced its outline. We then specified the outer and inner rims of the medulla by clicking on their starting and ending points, and Matlab generated ten equally spaced control points on each rim. These twenty control points were used to register the medulla to a common fan-shaped template. After registration, the sums of all pixel-by-pixel fluorescent intensities within medulla were used for Fig. 2e. For Fig. 2f, we pooled data into 10 evenly spaced bins along the proximal-distal axis (which do not exactly correspond to the 10 layers), and added the fluorescent intensities within each bin. The total signal intensity in each bin was then normalized to the overall sum.

Statistics

No statistical methods were used to determine sample sizes, but our sample sizes are similar to those generally employed in the field. Individual flies were randomly assigned to treatment groups. Data collection and analysis were not performed blind to the conditions of the experiments.

Upon publication, the flies will be deposited in Bloomington Stock Center, and the plasmids deposited in Addgene. A supplementary methods checklist is available.

Supplementary Material

Refer to Web version on PubMed Central for supplementary material.

Acknowledgments

We thank D. Luginbuhl for generating transgenic flies; R. Alfa, J. Cao, X. Dong, Y. Fisher, D.M. Gohl, M. Lin, S. Park, C. Ran, K. Shen, M. Silies, X. Wei, Z. Yang, and C. Zhou for advice and technical support; H.A. Dierick, G. Dietzl, T. Lee, A. Rajan, G.M. Rubin, J.W. Wang, M. Zeidler, and Bloomington Stock Center for fly strains; Addgene for plasmids; L. DeNardo, C.J. Guenther, T.J. Mosca, and X. Wang for critiques on the manuscript. X.J.G. is supported by an Enlight Foundation Interdisciplinary Fellowship. L.L. is an investigator of the Howard Hughes Medical Institute. This study was also supported by NIH grants R01-DC005982 (L.L.), R01-EY022638 (T.R.C.), and R01-DC013070 (C.J.P.), and a grant from Whitehall Foundation (C.J.P.).

References

1. Tsien RY. Fluorescence measurement and photochemical manipulation of cytosolic free calcium. *Trends in neurosciences*. 1988; 11:419–424. [PubMed: 2469158]
2. Looger LL, Griesbeck O. Genetically encoded neural activity indicators. *Curr Opin Neurobiol*. 2012; 22:18–23. [PubMed: 22104761]
3. Marella S, Mann K, Scott K. Dopaminergic modulation of sucrose acceptance behavior in *Drosophila*. *Neuron*. 2012; 73:941–950. [PubMed: 22405204]
4. Inagaki HK, et al. Visualizing neuromodulation in vivo: TANGO-mapping of dopamine signaling reveals appetite control of sugar sensing. *Cell*. 2012; 148:583–595. [PubMed: 22304923]
5. Nusbaum MP, Blitz DM, Swensen AM, Wood D, Marder E. The roles of co-transmission in neural network modulation. *Trends in neurosciences*. 2001; 24:146–154. [PubMed: 11182454]
6. Takemura SY, et al. A visual motion detection circuit suggested by *Drosophila* connectomics. *Nature*. 2013; 500:175–181. [PubMed: 23925240]
7. Sheng M, Greenberg ME. The regulation and function of c-fos and other immediate early genes in the nervous system. *Neuron*. 1990; 4:477–485. [PubMed: 1969743]
8. Reijmers LG, Perkins BL, Matsuo N, Mayford M. Localization of a stable neural correlate of associative memory. *Science*. 2007; 317:1230–1233. [PubMed: 17761885]
9. Koya E, et al. Targeted disruption of cocaine-activated nucleus accumbens neurons prevents context-specific sensitization. *Nature neuroscience*. 2009; 12:1069–1073. [PubMed: 19620976]
10. Guenther CJ, Miyamichi K, Yang HH, Heller HC, Luo L. Permanent genetic access to transiently active neurons via TRAP: targeted recombination in active populations. *Neuron*. 2013; 78:773–784. [PubMed: 23764283]
11. Kawashima T, et al. Functional labeling of neurons and their projections using the synthetic activity-dependent promoter E-SARE. *Nat Methods*. 2013; 10:889–895. [PubMed: 23852453]
12. Fujita N, et al. Visualization of neural activity in insect brains using a conserved immediate early gene, Hr38. *Current biology : CB*. 2013; 23:2063–2070. [PubMed: 24120640]
13. Masuyama K, Zhang Y, Rao Y, Wang JW. Mapping neural circuits with activity-dependent nuclear import of a transcription factor. *Journal of neurogenetics*. 2012; 26:89–102. [PubMed: 22236090]
14. Rhoads AR, Friedberg F. Sequence motifs for calmodulin recognition. *Faseb J*. 1997; 11:331–340. [PubMed: 9141499]
15. Luan H, Peabody NC, Vinson CR, White BH. Refined spatial manipulation of neuronal function by combinatorial restriction of transgene expression. *Neuron*. 2006; 52:425–436. [PubMed: 17088209]
16. Pfeiffer BD, et al. Refinement of tools for targeted gene expression in *Drosophila*. *Genetics*. 2010; 186:735–755. [PubMed: 20697123]

17. Nassel DR. Insulin-producing cells and their regulation in physiology and behavior of *Drosophila*. *Can J Zool*. 2012; 90:476–488.
18. Hamada FN, et al. An internal thermal sensor controlling temperature preference in *Drosophila*. *Nature*. 2008; 454:217–220. [PubMed: 18548007]
19. Peersen OB, Madsen TS, Falke JJ. Intermolecular tuning of calmodulin by target peptides and proteins: differential effects on Ca²⁺ binding and implications for kinase activation. *Protein science : a publication of the Protein Society*. 1997; 6:794–807. [PubMed: 9098889]
20. Potter CJ, Tasic B, Russler EV, Liang L, Luo L. The Q system: a repressible binary system for transgene expression, lineage tracing, and mosaic analysis. *Cell*. 2010; 141:536–548. [PubMed: 20434990]
21. Riabinina O, et al. Improved and expanded Q-system reagents for genetic manipulations. *Nat Methods*. 2015
22. Bloomquist BT, et al. Isolation of a putative phospholipase C gene of *Drosophila*, *norpA*, and its role in phototransduction. *Cell*. 1988; 54:723–733. [PubMed: 2457447]
23. Estes PS, Ho GLY, Narayanan R, Ramaswami M. Synaptic localization and restricted diffusion of a *Drosophila* neuronal synaptobrevin - Green fluorescent protein chimera in vivo. *Journal of neurogenetics*. 2000; 13:233. [PubMed: 10858822]
24. Wong AM, Wang JW, Axel R. Spatial representation of the glomerular map in the *Drosophila* protocerebrum. *Cell*. 2002; 109:229–241. [PubMed: 12007409]
25. Clark DA, Bursztyn L, Horowitz MA, Schnitzer MJ, Clandinin TR. Defining the computational structure of the motion detector in *Drosophila*. *Neuron*. 2011; 70:1165–1177. [PubMed: 21689602]
26. Gaudry Q, Hong EJ, Kain J, de Bivort BL, Wilson RI. Asymmetric neurotransmitter release enables rapid odour lateralization in *Drosophila*. *Nature*. 2013; 493:424–428. [PubMed: 23263180]
27. Friggi-Grelin F, et al. Targeted gene expression in *Drosophila* dopaminergic cells using regulatory sequences from tyrosine hydroxylase. *Journal of neurobiology*. 2003; 54:618–627. [PubMed: 1255273]
28. Alekseyenko OV, Lee C, Kravitz EA. Targeted manipulation of serotonergic neurotransmission affects the escalation of aggression in adult male *Drosophila melanogaster*. *PloS one*. 2010; 5:e10806. [PubMed: 20520823]
29. Cole SH, et al. Two functional but noncomplementing *Drosophila* tyrosine decarboxylase genes. *Journal of Biological Chemistry*. 2005; 280:14948–14955. [PubMed: 15691831]
30. Wu Q, et al. Developmental control of foraging and social behavior by the *Drosophila* neuropeptide Y-like system. *Neuron*. 2003; 39:147–161. [PubMed: 12848939]
31. Park D, Veenstra JA, Park JH, Taghert PH. Mapping Peptidergic Cells in *Drosophila*: Where DIMM Fits. *PloS one*. 2008; 3
32. Fridell YW, Sanchez-Blanco A, Silvia BA, Helfand SL. Targeted expression of the human uncoupling protein 2 (*hUCP2*) to adult neurons extends life span in the fly. *Cell metabolism*. 2005; 1:145–152. [PubMed: 16054055]
33. Joiner MA, Griffith LC. Mapping of the anatomical circuit of CaM kinase-dependent courtship conditioning in *Drosophila*. *Learn Mem*. 1999; 6:177–192. [PubMed: 10327242]
34. Shohat-Ophir G, Kaun KR, Azanchi R, Mohammed H, Heberlein U. Sexual deprivation increases ethanol intake in *Drosophila*. *Science*. 2012; 335:1351–1355. [PubMed: 22422983]
35. Geminard C, Rulifson EJ, Leopold P. Remote control of insulin secretion by fat cells in *Drosophila*. *Cell metabolism*. 2009; 10:199–207. [PubMed: 19723496]
36. Rajan A, Perrimon N. *Drosophila* cytokine unpaired 2 regulates physiological homeostasis by remotely controlling insulin secretion. *Cell*. 2012; 151:123–137. [PubMed: 23021220]
37. Crocker A, Shahidullah M, Levitan IB, Sehgal A. Identification of a neural circuit that underlies the effects of octopamine on sleep:wake behavior. *Neuron*. 2010; 65:670–681. [PubMed: 20223202]
38. Roeder T. Tyramine and octopamine: Ruling behavior and metabolism. *Annu Rev Entomol*. 2005; 50:447–477. [PubMed: 15355245]

39. Monastirioti M, Linn CE, White K. Characterization of *Drosophila* tyramine beta-hydroxylase gene and isolation of mutant flies lacking octopamine. *Journal of Neuroscience*. 1996; 16:3900–3911. [PubMed: 8656284]
40. Chen TW, et al. Ultrasensitive fluorescent proteins for imaging neuronal activity. *Nature*. 2013; 499:295–300. [PubMed: 23868258]
41. Kitamoto T. Conditional modification of behavior in *Drosophila* by targeted expression of a temperature-sensitive shibire allele in defined neurons. *Journal of neurobiology*. 2001; 47:81–92. [PubMed: 11291099]
42. Broughton SJ, et al. Longer lifespan, altered metabolism, and stress resistance in *Drosophila* from ablation of cells making insulin-like ligands. *Proceedings of the National Academy of Sciences of the United States of America*. 2005; 102:3105–3110. [PubMed: 15708981]
43. Schrodel T, Prevedel R, Aumayr K, Zimmer M, Vaziri A. Brain-wide 3D imaging of neuronal activity in *Caenorhabditis elegans* with sculpted light. *Nat Methods*. 2013; 10:1013–1020. [PubMed: 24013820]
44. Ma H, et al. gammaCaMKII shuttles Ca(2+)/CaM to the nucleus to trigger CREB phosphorylation and gene expression. *Cell*. 2014; 159:281–294. [PubMed: 25303525]
45. Fosque BF, et al. Neural circuits. Labeling of active neural circuits in vivo with designed calcium integrators. *Science*. 2015; 347:755–760. [PubMed: 25678659]
46. Schmidt D, Cho YK. Natural photoreceptors and their application to synthetic biology. *Trends in biotechnology*. 2015; 33:80–91. [PubMed: 25466878]
47. Bath DE, et al. FlyMAD: rapid thermogenetic control of neuronal activity in freely walking *Drosophila*. *Nat Methods*. 2014
48. Palmer AE, et al. Ca²⁺ indicators based on computationally redesigned calmodulin-peptide pairs. *Chemistry & biology*. 2006; 13:521–530. [PubMed: 16720273]
49. Zhou C, Rao Y, Rao Y. A subset of octopaminergic neurons are important for *Drosophila* aggression. *Nature neuroscience*. 2008; 11:1059–1067. [PubMed: 19160504]
50. Nassel DR, Winther AM. *Drosophila* neuropeptides in regulation of physiology and behavior. *Progress in neurobiology*. 2010; 92:42–104. [PubMed: 20447440]
51. Tian L, et al. Imaging neural activity in worms, flies and mice with improved GCaMP calcium indicators. *Nat Methods*. 2009; 6:875–881. [PubMed: 19898485]
52. Montigiani S, Neri G, Neri P, Neri D. Alanine substitutions in calmodulin-binding peptides result in unexpected affinity enhancement. *J Mol Biol*. 1996; 258:6–13. [PubMed: 8613992]
53. Bischof J, Maeda RK, Hediger M, Karch F, Basler K. An optimized transgenesis system for *Drosophila* using germ-line-specific phiC31 integrases. *Proceedings of the National Academy of Sciences of the United States of America*. 2007; 104:3312–3317. [PubMed: 17360644]
54. Berdnik D, Chihara T, Couto A, Luo L. Wiring stability of the adult *Drosophila* olfactory circuit after lesion. *The Journal of neuroscience : the official journal of the Society for Neuroscience*. 2006; 26:3367–3376. [PubMed: 16571743]
55. Sweeney LB, et al. Temporal target restriction of olfactory receptor neurons by Semaphorin-1a/PlexinA-mediated axon-axon interactions. *Neuron*. 2007; 53:185–200. [PubMed: 17224402]
56. Smith HK, et al. Inducible ternary control of transgene expression and cell ablation in *Drosophila*. *Development genes and evolution*. 1996; 206:14–24. [PubMed: 24173393]
57. Lai SL, Awasaki T, Ito K, Lee T. Clonal analysis of *Drosophila* antennal lobe neurons: diverse neuronal architectures in the lateral neuroblast lineage. *Development*. 2008; 135:2883–2893. [PubMed: 18653555]
58. Hombria JC, Brown S, Hader S, Zeidler MP. Characterisation of Upd2, a *Drosophila* JAK/STAT pathway ligand. *Developmental biology*. 2005; 288:420–433. [PubMed: 16277982]
59. Monastirioti M, Linn CE Jr, White K. Characterization of *Drosophila* tyramine beta-hydroxylase gene and isolation of mutant flies lacking octopamine. *The Journal of neuroscience : the official journal of the Society for Neuroscience*. 1996; 16:3900–3911. [PubMed: 8656284]
60. Katsov AY, Clandinin TR. Motion processing streams in *Drosophila* are behaviorally specialized. *Neuron*. 2008; 59:322–335. [PubMed: 18667159]

61. Kim DE, Chivian D, Baker D. Protein structure prediction and analysis using the Robetta server. *Nucleic Acids Res.* 2004; 32:W526–W531. [PubMed: 15215442]
62. Wu JS, Luo L. A protocol for dissecting *Drosophila melanogaster* brains for live imaging or immunostaining. *Nature protocols.* 2006; 1:2110–2115. [PubMed: 17487202]

Author Manuscript

Author Manuscript

Author Manuscript

Author Manuscript

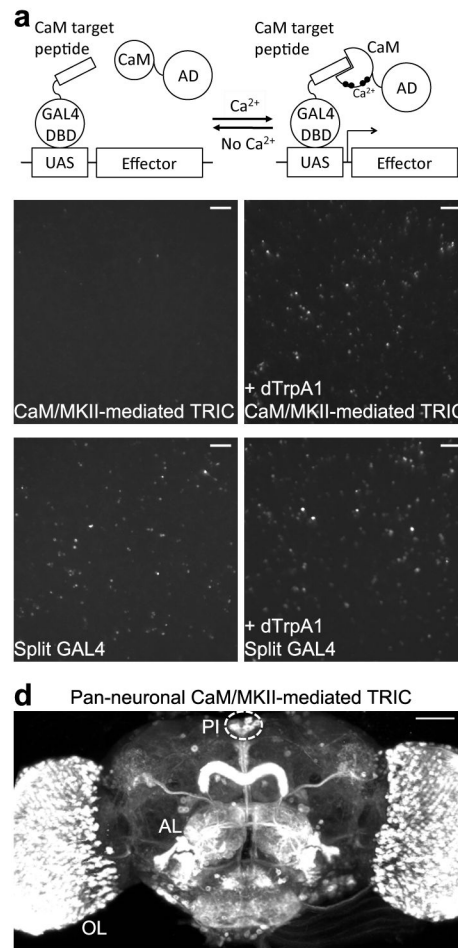


Figure 1. Proof-of-principle of transcriptional reporter of intracellular Ca^{2+} (TRIC) in cultured cells and transgenic flies

(a) The design of TRIC. Ca^{2+} mediates the binding of calmodulin (CaM) and its targeting peptide, thus bringing a transcriptional activation domain (AD, fused with CaM) to the DNA-binding domain (DBD) of a transcription factor (here yeast GAL4, fused with CaM-targeting peptide), and activating transcription of an effector that is under the control of UAS. The binding of two fusion proteins depends on Ca^{2+} concentration. (b) CaM/MKII-mediated TRIC (*ActP-MKII::GAL4DBD*, *ActP-p65AD::CaM*). The *UAS-GFP* expression (right) is much weaker and sparser in the absence of *ActP-dTrpA1* (left). (c) Split GAL4s that bind constitutively via leucine zippers (Zp) were used as a positive control (*ActP-Zp::GAL4DBD*, *ActP-VP16AD::Zp*). The *UAS-GFP* expression is independent of *ActP-dTrpA1*. Cells in **b c** have all been subjected to the same repetitive heat shocks. (d) CaM/MKII-mediated TRIC signal in the brain of transgenic flies (*nsyb-MKII::GAL4DBD*, *QUAS-p65AD::CaM*, *nsyb-QF2*, *tubP-QS*, *UAS-mCD8::RFP*, representative of 10 samples). OL, optic lobe; AL, antennal lobe; PI, *pars intercerebralis* cells (dashed circle). In this and subsequent figures, unless specified, the maximal projections of confocal image stacks are shown, and the scale bars represent 50 μm .

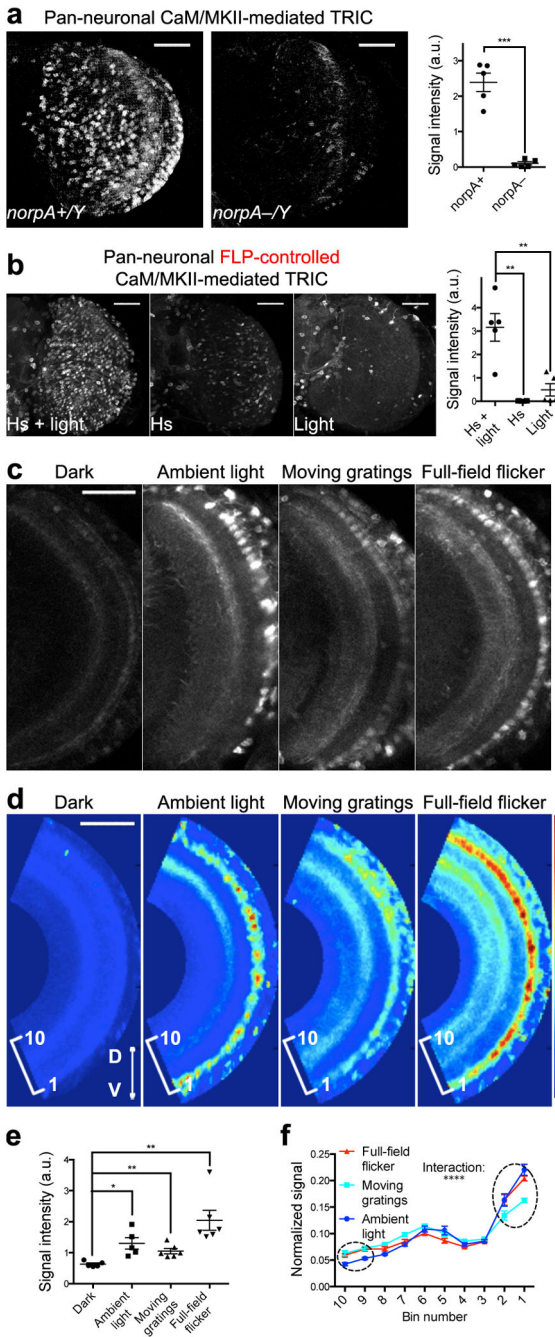


Figure 2. TRIC signals in the optic lobes depend on visual transduction and visual experience
(a) TRIC signal in the optic lobes is diminished in *norpA* mutants, in which phototransduction was blocked (Genotype besides *norpA*: *nsyb-MKII::GAL4DBDo*, *QUAS-p65AD::CaM*, *nsyb-QF2*, *tubP-QS*, *UAS-mCD8::GFP*, n = 5). **(b)** In this experiment, a core TRIC component, *p65AD::CaM*, is conditionally expressed upon FLP-mediated recombination, which is in turn controlled by heat-shock (*nsyb-MKII::GAL4DBDo*, *QUAS-FRT-stop-FRT-p65AD::CaM*, *hsFLP122*, *nsyb-QF2*, *UAS-mCD8::GFP*, n = 5). The optic lobe exhibits strong TRIC signal in response to light exposure after heat-shock (hs)

induction. TRIC signal diminishes in the absence of light (“hs”) or heat-shock (“light”). (**c–f**) Visual experiences modulate TRIC signals in the medulla ($n = 5$, same genotype as in **b**). Shown are representative sections (**c**), the heat maps of average TRIC signals (**d**, color scale 0–255), total fluorescence quantification (**e**), and relative light-induced signal intensity in 10 evenly spaced bins (**f**) where circles highlight bins show significant difference between different stimulations. Two-tailed unpaired t-test for **a** ($p = 0.0007$), **b** ($p = 0.0061, 0.0074$), and **e** ($p = 0.0209, 0.0027, 0.0069$), with Holm-Bonferroni correction for multiple comparisons; two-one ANOVA for **f** (interaction $p < 0.0001$), with Tukey post hoc comparisons. In this and subsequent figures, * $P < 0.05$, ** $P < 0.01$, *** $P < 0.001$, **** $P < 0.0001$; the data are presented as scatter dots with mean \pm s.e.m.; the representative images correspond to the medians; key changes of genetic components are colored red.

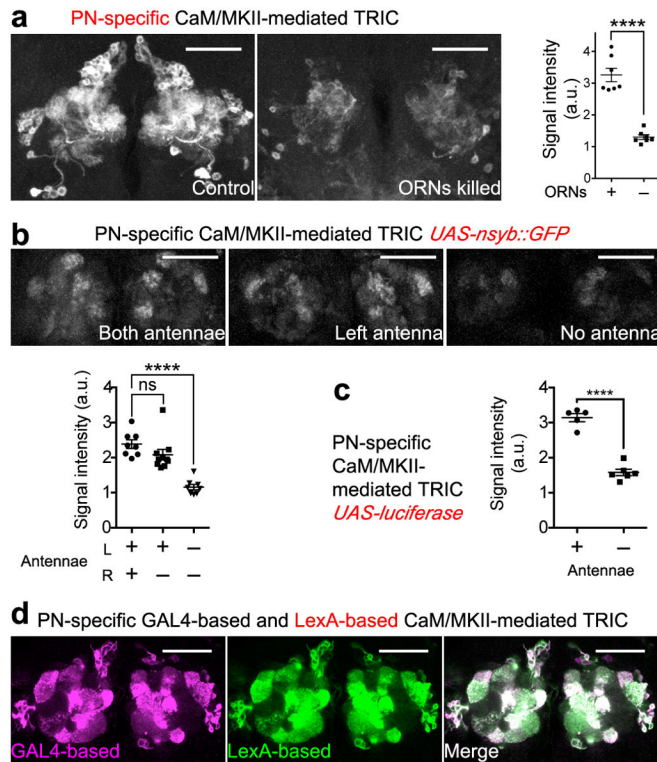


Figure 3. Characterization of TRIC in olfactory projection neurons (PNs)

(a) Genetic ablation of ORNs reduces TRIC signal in PNs (*nsyb-MKII::GAL4DBDo*, *QUAS-p65AD::CaM*, *GH146-QF*, *UAS-mCD8::GFP*; n = 7). In “ORNs killed”, expression of ricin toxin A (RTA) is restricted to the ORNs (+ *peb-GAL4*, *ey-FLP*, *UAS-FRT-w+-FRT-RTA*), where the *ey* enhancer expresses FLP to remove *w+*, and the *peb-GAL4* drives RTA expression in ORNs. (b) Bilateral but not unilateral antenna removal reduces TRIC signal, using *nsyb::GFP* as the reporter (*nsyb-MKII::GAL4DBDo*, *QUAS-p65AD::CaM*, *GH146-QF*, *UAS-nsyb::GFP*; n = 8). (c) A luciferase reporter detects the reduction of TRIC signal by antenna removal (n = 5). (d) Similarity in PN labeling between GAL4-based and LexA-based TRICs (*nsyb-MKII::GAL4DBDo*, *nsyb-MKII::nlsLexADBDDo*, *QUAS-p65AD::CaM*, *GH146-QF*, *UAS-mCD8::RFP*, *lexAop2-mCD8::GFP*, representative of 10 brains). Shown are single confocal slices. Two-tailed unpaired t-test for **a** ($p < 0.0001$), **b** ($p = 0.1384$, < 0.0001), and **c** ($p < 0.0001$), with Holm-Bonferroni correction for multiple comparisons.

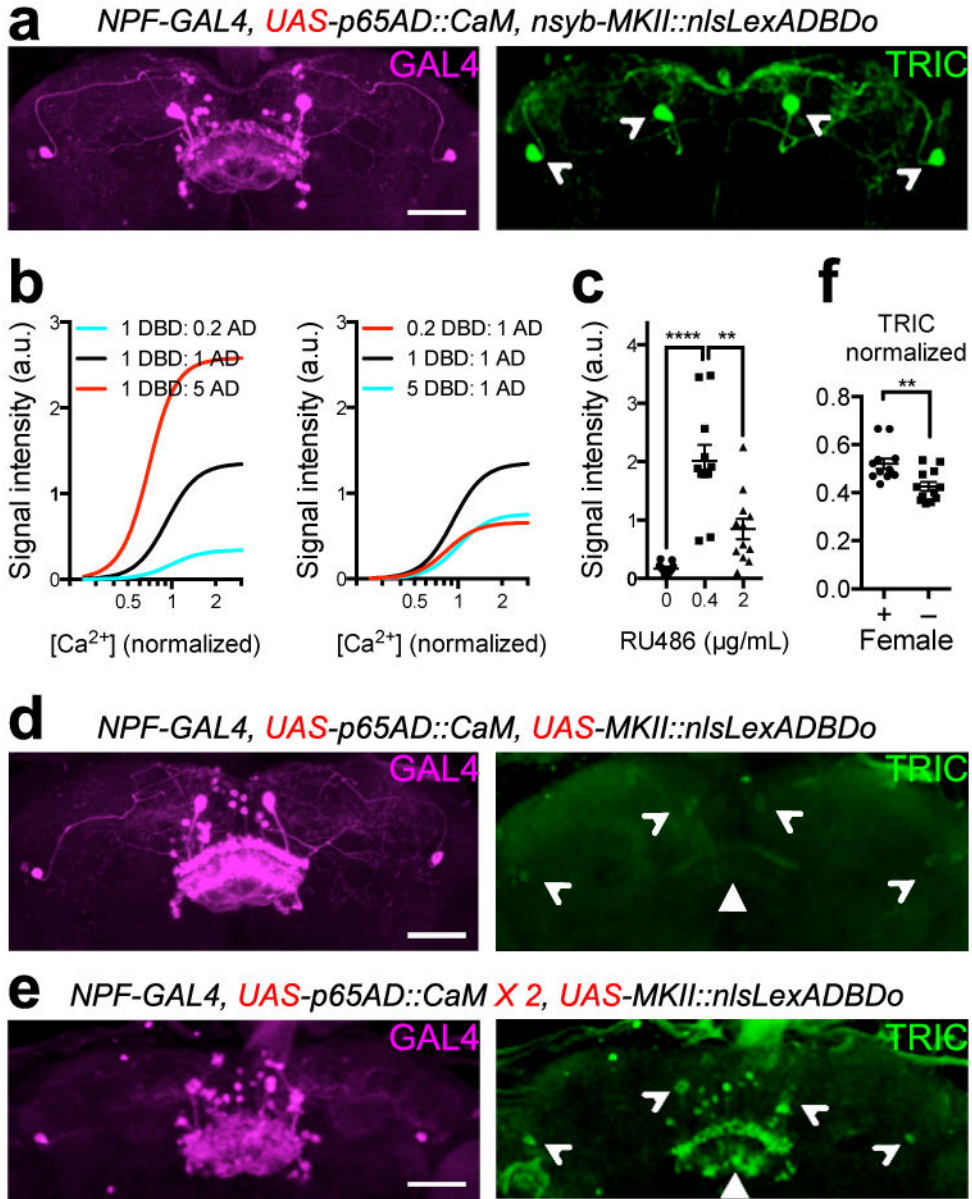


Figure 4. Stoichiometric tuning of TRIC and its application in NPF neurons

(a) Monitoring NPF neurons using LexA-based TRIC (*nsyb-MKII::nlsLexADBD0, UAS-p65AD::CaM, npf-GAL4, UAS-mCD8::RFP, LexAop2-mCD8::GFP*, representative of 6 samples). The GAL4 expression is visualized with RFP (left); the arrowheads indicate the only four cells with prominent TRIC signal (right). (b) Simulating effects of DBD/AD stoichiometry on TRIC signal. Increasing AD dose increases signal (left), whereas increasing DBD dose first increases and then decreases signal (right). (c) Validating the scenario in (b, left) with PI cells (*UAS-MKII::nlsLexADBD0, ilp2-GeneSwitch, QUAS-p65AD::CaM, nsyb-QF2, tubP-QS, UAS-mCD8::RFP, LexAop2-mCD8::GFP*, n = 11). Increasing GeneSwitch-mediated DBD expression with RU486 first increases and then decreases TRIC signal. (d–e) Tuning NPF TRIC signal with more balanced expression of

DBD/AD (*UAS-MKII::nlsLexADBDo*, *UAS-p65AD::CaM* [$\times 1$ in **d**; $\times 2$ in **e**], *npf-GAL4*, *UAS-mCD8::RFP*, *LexAop2-mCD8::GFP*, representative of 6 samples). The arrowheads indicate the same cells as in **(a)**, and the triangles indicate the additional signal in the fan-shaped body. **(f)** Ratiometric TRIC measurement reveals that sexual deprivation lowers Ca^{2+} activity in male NPF neurons in the fan-shaped body ($n = 12$, same genotype as in **e**). Two-tailed unpaired t-test for **c** ($p < 0.0001$, $\rho = 0.0022$) and **f** ($p = 0.0033$), with Holm-Bonferroni correction for multiple comparisons.

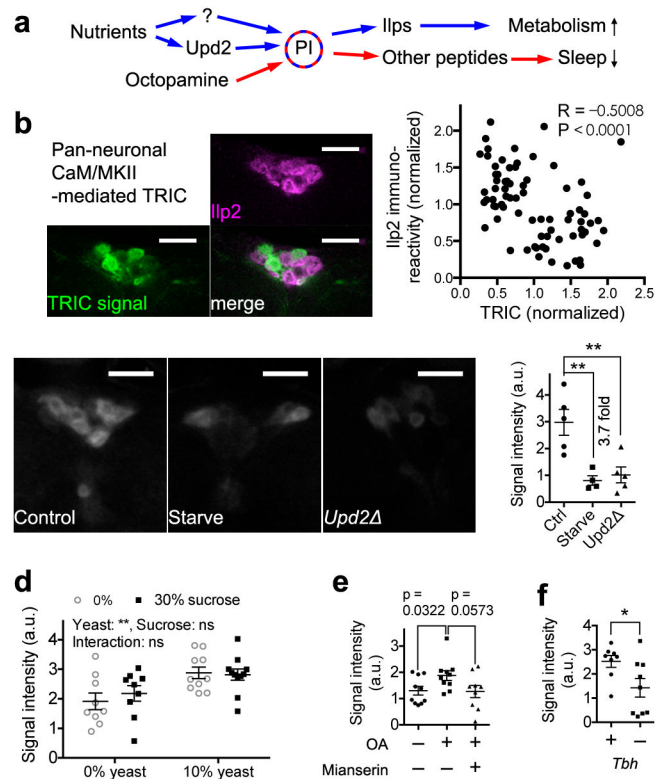


Figure 5. Monitoring PI cell activity with TRIC

(a) Summary of two known pathways regulating PI activity. Our data suggest an unknown pathway in parallel to Upd2 from nutrients to PI. (b) TRIC signal in the PI cells negatively correlates with the intensity of Ilp2 staining. Shown are single confocal slices. Spearman's rank correlation for the quantification, where each dot represents one cell after normalizing it to the mean value in the corresponding animal. (c) Compared to wild-type flies on regular food ("control"), TRIC signal in the PI is reduced by food deprivation ("starve") or hemizygous *upd2* deletion ($n = 4$). 20 mg QA per vial was used to induce TRIC expression. (d) Yeast but not sucrose increases TRIC signal ($n = 8$). (e) 10 mg/mL OA increases TRIC signal, which is antagonized by 2 mg/mL mianserin, an OA antagonist ($n = 9$). (f) TRIC signal is reduced by hemizygous *tbh* mutation, which eliminates an enzyme necessary for OA synthesis ($n = 8$). All panels are of the same genotype as Fig. 1d, except for c and f where *mCD8::RFP* is replaced with *mCD8::GFP*. Two-tailed unpaired t-test for c ($p = 0.0041, 0.0057$), e ($p = 0.0032, 0.0573$), and f ($p = 0.0313$), with Holm-Bonferroni correction for multiple comparisons. Two-way ANOVA for d. Scale bar, 20 μm .

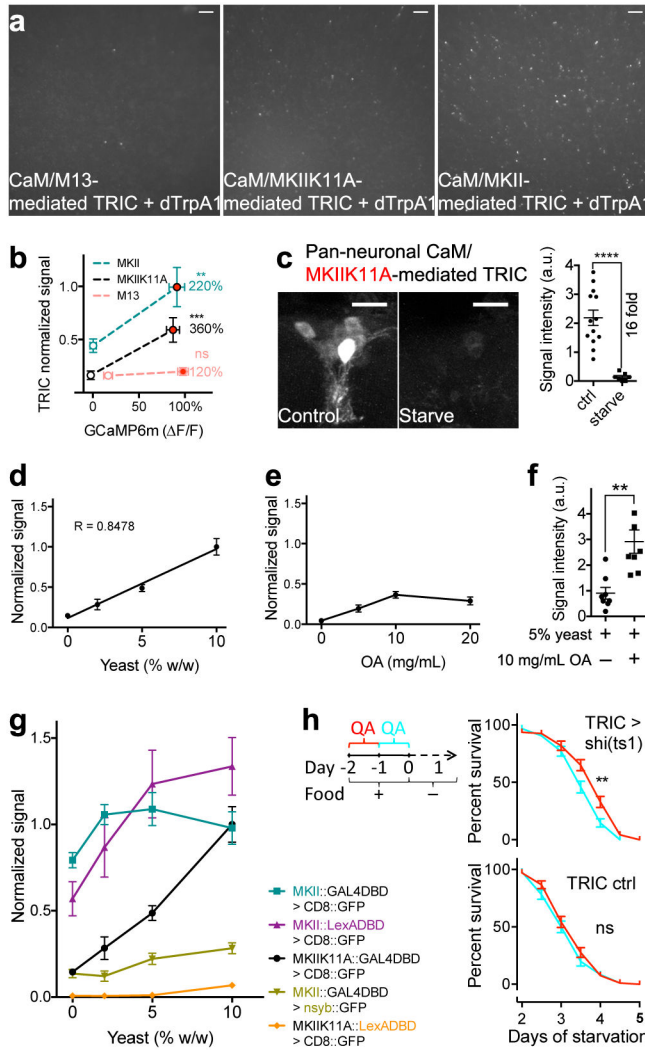


Figure 6. Improved signal/noise using mutant TRIC components allows quantitative analysis and manipulation of PI cells
 (a) In S2 cells, the K11A variant of MKII generates reporter expression at a level in between M13 and MKII in the presence of dTrpA1. The experiments are as in Fig. 1b except for the specific CaM-target peptides. (b) Simultaneous quantification of TRIC and GCaMP6m signals in S2 cells, in the presence (red-filled dots) or absence (open dots) of dTrpA1. “TRIC normalized signal” is the fluorescent intensity of tdTomato expressed by TRIC divided by the baseline fluorescent intensity of GCaMP6m. Of the three variants, MKIIK11A shows the largest fold of TRIC signal induction (n = 189 cells for each condition). The fold of TRIC signal induction in experimental conditions (with dTrpA1) was labeled in percentage of control (no dTrpA1), as a direct comparison to the scale of $\Delta F/F$. (c) TRIC signal shows higher fed-to-starved ratio with MKIIK11A (n = 7, compared to Fig. 5c). (d) TRIC signal varies linearly with yeast concentration (n = 9), showing the Pearson correlation between yeast concentration and the mean TRIC signal at every concentration. (e) TRIC signal plateaus as OA concentration increases (n = 9). (f) In the presence of 5% yeast, 10 mg/mL OA further increases TRIC signal (n = 8). (g) Signals of different TRIC

variants in response to varying yeast concentrations (n = 10 for each data point). All data are normalized to the signal of MKI1K11A::GAL4DBDo driving mCD8::GFP, exposed to 10% yeast; MKI1K11A::GAL4DBDo data are re-plotted from **(d)**. **(h)** Left, experimental setup. Under the experimental (red) or control (cyan) condition, flies were treated with QA 1–2 or 0–1 days before the onset of starvation (at day 0). Top right, flies with PI-activity-dependent expression of *shi^{ts1}* using TRIC (TRIC > *shi^{ts1}*) have extended longevity during starvation in the experimental condition (red) compared to control condition (cyan) (upper panel, n = 94 flies). Bottom right, flies with TRIC transgenes without *shi^{ts1}* do not exhibit a difference between the experimental and control conditions (lower panel, n = 96 flies). Base genotype **(c–f)**: *nsyb-MKI1K11A::GAL4DBDo*, *QUAS-p65AD::CaM*, *nsyb-QF2*, *tubP-QS*, *UAS-mCD8::RFP/GFP*; **g**: colored components were used to replace corresponding transgene the base genotype; **h**: *mCD8::GFP* in the base genotype was replaced with *shi^{ts1}*. Two-tailed unpaired t-test for **b** (p = 0.005, 0.0005, 0.4114), **c** (p < 0.0001), and **f** (p = 0.0072) with Holm-Bonferroni correction for multiple comparisons. Log-rank test for **h** (p = 0.0012, 0.3411). Scale bar for PI cells, 20 μm.